



A Modified Multi-Level Tracking Scheme for the Detection of Sunspot Umbral Dots

ROHAN EUGENE LOUIS ¹ AND AMIT CHATURVEDI ¹

¹*Udaipur Solar Observatory, Physical Research Laboratory, Dewali Badi Road, Udaipur –313001, Rajasthan, India*

ABSTRACT

Umbral dots (UDs) are small-scale convective intrusions in the umbral core of sunspots and pores. Different methods have been used in the past to determine the physical properties of UD. One of the methods typically used is multi-level tracking (MLT), which tags spatial structures at equi-spaced intensity levels from the highest level while progressing downward. A modified approach to the regular MLT is explored in this article that also uses the local intensity maxima with a change in the threshold condition to enclose a UD, such that diffuse UD do not appear extended than they visually appear. The physical properties of UD from these two MLT approaches are compared. The methods are implemented on high-resolution blue continuum images of four sunspots from the 50-cm Solar Optical Telescope on board *Hinode*. In addition, we introduce a density-based, spatial clustering routine for the first time to ascertain the differences resulting from the two tracking methods. The modified MLT approach yields an effective diameter with median values ranging from 250–310 km which is on average 70–90 km smaller than the regular MLT approach. The lower effective diameter in the modified method is associated with a reduced UD fill fraction of 12%–13% while the regular method yields 17–19%. However, these differences are still within the range of values cited by earlier works. On the other hand, the histogram of the mean intensity of UD from both methods is nearly identical. The spatial clustering of UD from both methods also shows very similar results. There is, however, a preferential spatial concentration of UD, particularly at locations where the umbral core is highly irregular and in the vicinity of faint light bridges. The dependency of the localized clustering of UD on the evolutionary phase of the sunspot and its magnetic complexity needs to be further explored.

Keywords: Sunspots (1653) — Solar Magnetic Fields (1503) — Solar Photosphere (1518)

1. INTRODUCTION

Sunspots are locations of intense magnetic fields where the photospheric magnetic field strength is in excess of 2.5 kG. The presence of strong magnetic fields suppresses overturning convective motions within sunspots (L. Biermann 1941; S. M. Chitre 1963), rendering their appearance to be darker than the surrounding quiet-Sun (QS). While the umbra is the darkest region of a sunspot, the emitted energy is still 10–20% of that in the QS, which cannot be carried solely by radiation. This surplus brightness is the result of convective motions that are greatly reduced in the presence of strong magnetic fields (W. Deinzer 1965), and is associated with umbral dots (UDs) – sub-arcsecond, bright features that populate the dark umbral background (R. E. Danielson 1964; J. M. Beckers & E. H. Schröter 1968; R. E. Loughhead et al. 1979).

UDs can be considered as either intrusions of hot, non-magnetized plasma within the “gappy” umbral magnetic field (E. N. Parker 1979; A. R. Choudhuri 1986), or oscillatory convection in thin columns of a monolithic sunspot (N. O. Weiss et al. 1990). Three-dimensional radiative magneto-hydrodynamic (MHD) simulations of magneto-convection by M. Schüssler & A. Vögler (2006) depict UD as narrow, convective plumes, which radiatively cool near the continuum-forming height. The UD appear as elongated structures, with a central dark lane that coincides with strong upflows that are flanked by relatively weaker downflows. The fine structure in UD, as predicted by numerical simulations, has been observationally verified and described in T. Rimmele (2008); M. Sobotka & K. G. Puschmann (2009); A. Ortiz et al. (2010).

UDs are generally categorized as “central” and “peripheral” (U. Grossmann-Doerth et al. 1986) structures based on their relative location in the umbra and have intensities of about $0.34 I_{QS}$ and $0.48 I_{QS}$, respectively (M. Sobotka et al. 1997a; A. Tritschler & W. Schmidt

2002), while T. L. Riethmüller et al. (2008) reported values of $0.53 I_{\text{QS}}$ and $0.65 I_{\text{QS}}$, respectively. On the other hand, the ratio of the peak-to-background intensity is about 1.15 for central UDs and about 1.23 for peripheral ones (T. L. Riethmüller et al. 2008), while H. Watanabe et al. (2012) reported values of about 1.46 and 1.5, respectively. In general, larger and long-lived UDs are seen in areas of enhanced background intensity (M. Sobotka et al. 1997b). The sizes of UDs can range from 125 km to 400 km, as reported by various authors using different identification routines (M. Sobotka et al. 1997b; A. Tritschler & W. Schmidt 2002; M. Sobotka & K. G. Puschmann 2009; M. Sobotka & J. Jurčák 2009; H. Watanabe et al. 2009; R. E. Louis et al. 2012; H. Watanabe et al. 2012). UDs typically fill around 6–18% of the umbral area (M. Sobotka et al. 1997b; A. Tritschler & W. Schmidt 2002; R. Yadav et al. 2018).

The differences in values of the physical properties can be attributed to the various techniques utilized in the identification of UDs as well as the type of sunspot analyzed. These detection methods include, edge enhancement with thresholding (M. Sobotka et al. 1997b), low-noise curvature detection (H. Hamedivafa 2008; M. Sobotka & K. G. Puschmann 2009), intensity thresholding (H. Watanabe et al. 2009), and multi-level tracking (MLT; T. L. Riethmüller et al. 2008; L. Bharti et al. 2010; R. E. Louis et al. 2012; R. Yadav et al. 2018). In this article, we implement MLT and a modified version of it, which uses the local intensity maxima and an altered threshold, on a set of four sunspots to determine the differences in the size, peak-to-background ratio, and fill fraction. We also introduce a density-based clustering routine for the first time to sort UDs on the basis of their spatial positions and ascertain the differences arising from the two tracking schemes. The rest of the article is organized as follows: Sect. 2 summarizes the observations, while Sect. 3 describes the detection and clustering techniques. The results are presented in Sect. 4. The discussion and conclusions are presented in Sects. 5 and 6, respectively.

2. OBSERVATIONS

We utilize high-resolution blue continuum filtergrams from the 50-cm Solar Optical Telescope (S. Tsuneta et al. 2008) on board the Japanese satellite *Hinode* (T. Kosugi et al. 2007). The filtergrams have a spatial sampling of $0''.109$ and were taken with a broad-band filter with a width of 4 \AA and centered at 450.45 nm. The four sunspots analyzed in this study are NOAA AR 10923, 10933, 10953, and 11330, which were observed by *Hinode* on 2006 November 14, 2007

January 05, 2007 May 02, and 2011 October 27, respectively. The four sunspots were located at a heliocentric angle of 8° , 2° , 16° , and 2° , respectively. The Level-0 data were processed to Level-1 data using the “*fg-prep*” routine in SolarSoft, which carried out dark correction, flat-fielding, and removal of bad pixels. The average QS was then used to normalize the images. To extract the umbra-penumbra boundary, we used the Otsu’s histogram shape-based, image thresholding technique (N. Otsu 1979; P.-S. Liao et al. 2001) and smoothed the resulting contour by 11 pixels. Even though UDs are highly dynamic, we analyzed a single image for each sunspot as we were interested in the differences from the two detection schemes. The use of multiple sunspots ensured that the distinct morphology, evolutionary epoch, and area of the four active regions rendered the analysis equivalent to a frame by frame comparison for a time series dataset. Figure 1 shows the sunspots analyzed in this article.

3. DATA ANALYSIS

3.1. Multi-Level Tracking (MLT)

MLT (B. Bovelet & E. Wiehr 2001) is a method that involves splitting the intensity levels in an image into equi-spaced values and tracking structures from the top-most intensity level to the bottom-most level, tagging features as they appear at each level to either previously detected structures or new features that appear for the first time at that level. The one-dimensional and two-dimensional illustrations of MLT are described in T. L. Riethmüller et al. (2008) and R. E. Louis et al. (2012), respectively. Prior to implementing MLT on each sunspot image, we determined the local intensity maximum and minimum within a 5×5 pixel neighbourhood, whose values are shown in Fig. 2. The general distribution of intensity values shows that 60% of the points (78% in the case of AR 10923) are faint and diffuse. The minimum intensity within the umbra is indicated by the gray line, while the blue line is 30% higher than the minimum value and is chosen as the new minimum intensity level in the umbra for MLT. The reason for choosing a 30% threshold is to avoid spurious or noisy structures from being identified by MLT, as lower intensities correspond to the darkest regions of the umbra that are generally devoid of any features that can be resolved. In addition, the local maxima detection routine picks up points that have the highest value in the neighborhood, irrespective of the intrinsic intensity of that patch in the umbra. The mean value of all local intensity maxima, exceeding the minimum value, is indicated by the red line. The range of the mean values lie between 0.15 in AR 10923 to 0.35 in AR 10933. We

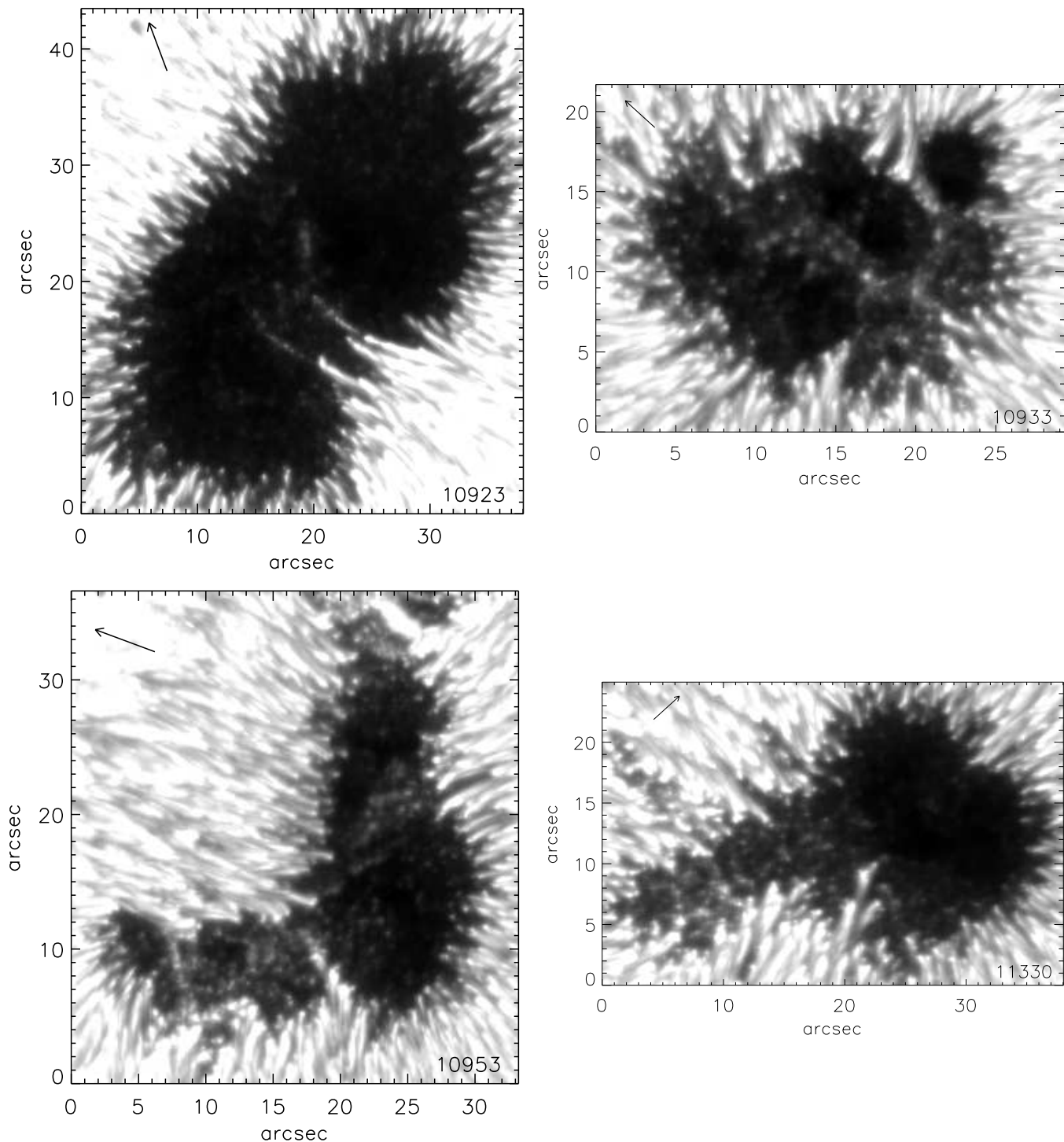


Figure 1. Sunspot umbrae analyzed in this work. The NOAA AR is inscribed in the bottom-right corner, while the arrow in the top-left corner points to disk center. The images have been clipped in intensity to show the detail within the umbra.

choose the pixels of local intensity maxima that have values between the red and the blue lines in the figure and save their spatial position. Once MLT completes indexing all features in the umbra, the selection

of the feature in each indexed patch is done using the mean of the maximum intensity and background intensity, i.e., $0.5 * (I_{\max} + I_{\text{bck}})$, which yields a contour around the feature. The background intensity is an image that

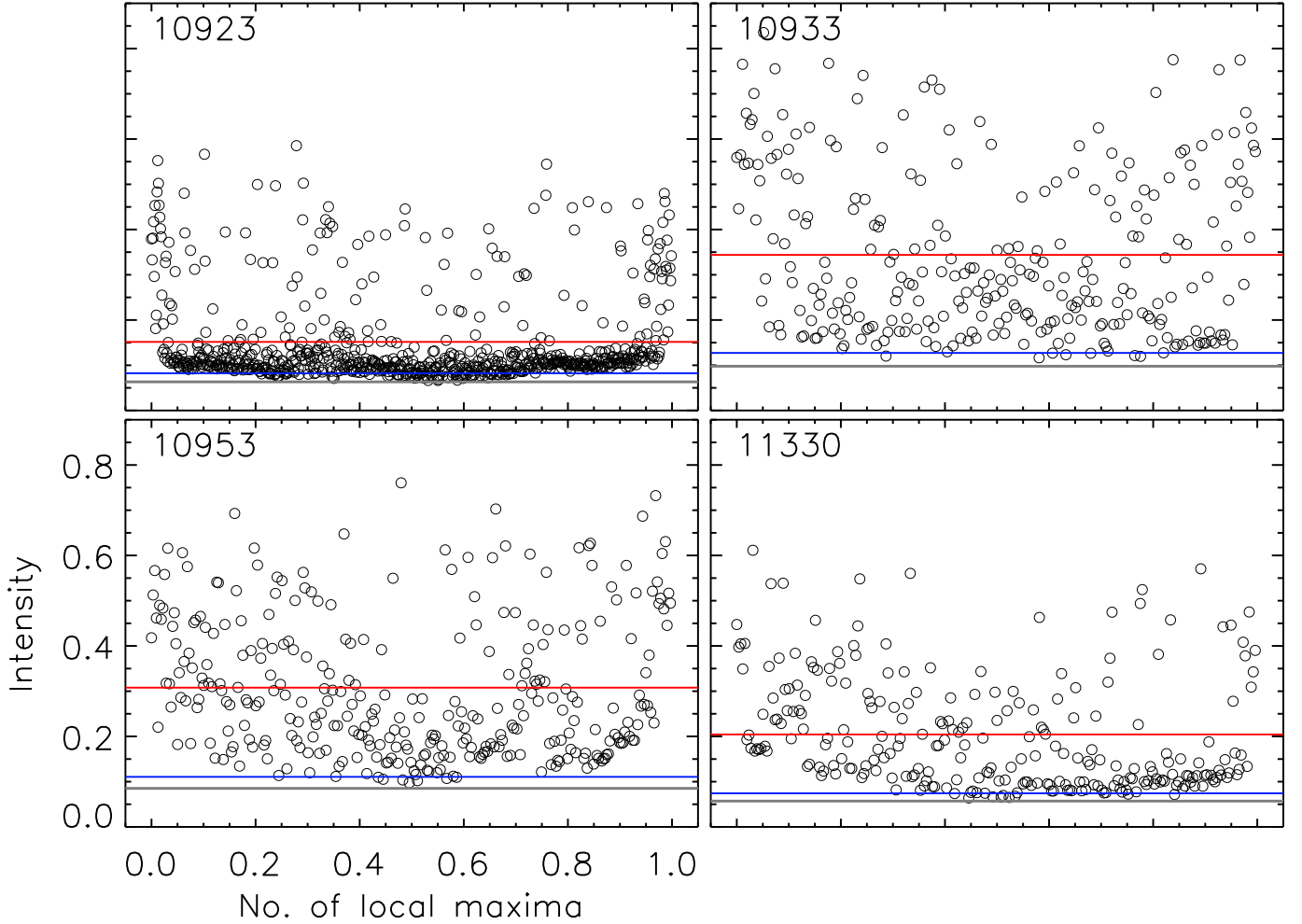


Figure 2. The intensity at the locations of the local maximum within the umbra shown with open circles. The gray line depicts the minimum intensity level (I_{\min}) within the umbra, the blue line at $1.3I_{\min}$, and the red line marks the mean value of intensity greater than $1.3I_{\min}$.

is devoid of UDs and is determined using the procedure described in I. Barrodale et al. (1993). The area enclosed by the contour is calculated with the boundary points using the ‘shoelace method’ (A. L. F. Meister 1769), which is based on the ‘triangle method’, wherein $A = 0.5|\sum_{i=1}^n(x_i y_{i+1} - x_{i+1} y_i)|$, with $(x_{n+1}, y_{n+1}) = (x_1, y_1)$. The area within the contour should exceed four pixels, and the contour should have a two-pixel separation from the umbra-penumbra boundary. The corresponding contour outlining the feature is indexed, labeled “A”, and the coordinates saved. The region enclosed by the contour is set to one in a binary map, which is repeated for each indexed region detected by MLT. If the contour encloses points of local maxima, then the contour label is changed to “B”. We utilize the “ray-casting”² procedure to determine if our point of

local maximum is within the contour or not. A separate list is created for those local maxima points that do not have any contour enclosing them. The reason the residual local maxima points lack a contour around them is due to the threshold of the mean value between the maximum and background intensity used by MLT. In an additional step, hereafter referred to as stage-2, we center a circle on the point having the local maximum with a 3-pixel radius and determine which pixels are assigned a value of zero from the previously created binary image for the MLT contours. The contour is determined around the local maximum point using a level equal to the mean value between the maximum and minimum intensity and is saved if the area is greater than four pixels. The contours determined in stage-2 are assigned a label “C”.

In the modified scheme, we implement MLT as before, but we check if the patch contains points of local maximum. If there are no points of local maximum, then the

² <https://www.youtube.com/watch?v=TA8XQgiao4M>

contour is saved and labeled “A” as in the regular case, ensuring that the area exceeds 4 pixels. If the patch contains points of local maximum, then all contours within the patch, having a threshold exceeding 50% of the sum of maximum intensity and mean intensity in the patch, i.e., $0.5 * (I_{\max} + I_{\text{mean}})$, are determined and saved if their area exceeds 4 pixels. This set of contours is labeled “B”. The reason for using a different threshold in the modified approach is to prevent diffuse or faint structures to become more extended than they appear visually. The above process is repeated until all the patch indices from MLT have been checked. The remaining points of local maximum that are not enclosed by a contour are subjected to stage-2 processing, as described earlier for the regular MLT scheme. To summarize, the regular and modified schemes differ in the manner in which “B”-labeled contours are determined, with distinct threshold values for both methods that produce a single contour in the former approach and multiple contours in the latter.

3.2. Clustering of UDs

While several clustering routines are available for sorting multi-dimensional datasets, *k-means* is the most widely used unsupervised scheme, particularly in solar physics for grouping spectral profiles (B. Viticchié & J. Sánchez Almeida 2011; A. Sainz Dalda et al. 2019; R. E. Louis et al. 2024). Given the number of clusters, *k-means* utilizes Euclidean distances between the data points and a set of initial random cluster centers to assign each point to a cluster based on the minimum distance. At the end of each iteration, the centroids of each cluster are updated, and the sorting continues until the cluster centroid and the variance of each cluster stabilize. The advantages of *k-means* are its simplicity, speed, and effectiveness to handle large, high-dimensional datasets. However, given its centroid-based implementation, it fails in situations where there are outliers in the data and if the clusters have different sizes or densities. This is particularly seen in the sunspot umbral core, where either one or all the following conditions may exist, such as the absence of UDs in the dark nuclei of the umbra, clumps of UDs appearing close to the umbra-penumbral boundary, or large-scale clustering of UDs forming faint light bridges. In this article, we utilize a Density Based Spatial Clustering of Applications with Noise (DBSCAN) for grouping UDs that were detected from the two MLT schemes using the centroid positions derived from the various contour labels. DBSCAN can deal with outliers, datasets with varying densities, and does not require a number of clusters to sort the data into, like its counterpart *k-means*. However, it requires two parameters,

namely, the radius or eps circle (ϵ) and the min points (M). The clustering works by segregating points into core, border, and noise points in the following manner. A core point is one that contains points greater than or equal to M within a circle of radius ϵ centered on it. All other points that do not satisfy the above condition are labeled noise points initially. In order to assign a cluster number to all the core points and separate the border points from noise points, the first core point is assigned an index one, and all points within its ϵ circle are also assigned the same index. We will refer to this as Step-1. A separate list is created with those points within this ϵ circle that are assigned an index one and checked one-by-one if they are core points or border points. We will refer to this as Step-2. If a core point is encountered, i.e., there are points greater than or equal to M in the ϵ circle, then these additional points are assigned an index one and added to the list described above. If there are less than M points, the point is a border point. It is labeled as such, but no further points in its ϵ circle are added to the list. In either case, a flag is set to indicate that this point has been verified and the program will exclude it when accessing the list containing points with an index one. Step-2 is repeated until all the points in the list with an index one, which are yet to be verified, have been exhausted. The index is then incremented to two, and Step-1 is repeated over all remaining core points that have not been assigned an index. In this manner, one obtains several clusters consisting of core and border points, as well as a number of noise points/outliers. This entire routine was written in the Interactive Data Language³ and verified with the standard “DBSCAN” function in Python, which is part of the “Scikit-learn” library.

4. RESULTS

4.1. Spatial Distribution of UDs

Figures 3–6 show the identified UDs in the different sunspots using the regular (left) and modified (right) MLT scheme. The red contours are common to both schemes and primarily trace brighter UDs that lie near the umbra-penumbral boundary as well as in the extended structures such as light bridges. This is due to the criteria set for the contours labeled “A”, which do not enclose any points of maximum intensity in the local neighborhood. The UDs enclosed by the red contours account for nearly half the total number in ARs 10933, 10953, and 11330 using both detection schemes, while it is around 30% for AR 10923. The number of

³ <https://github.com/Rohan-Louis-81/IDL>

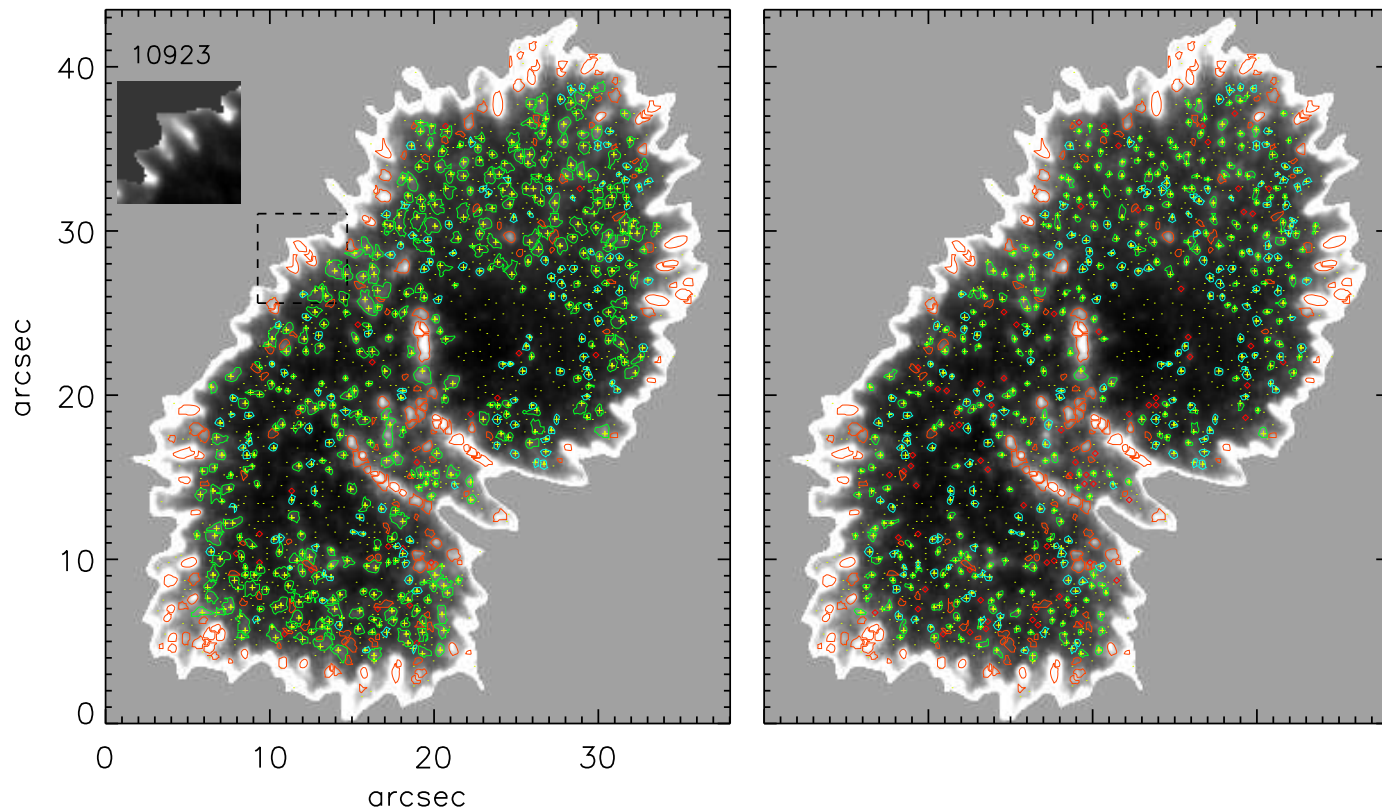


Figure 3. Identification of UDs using the MLT scheme for AR 10923. The red contours outline UDs that do not contain a pixel with a local maxima. The green contours are those that contain a local maxima indicated with a yellow plus symbol. The cyan contours enclose those local maxima that were undetected, while the red diamonds represent locations of local maxima without a contour. The yellow dots represent locations of local minima. The left and right panels correspond to UDs identified using the regular MLT and modified MLT technique, respectively. See the text for an explanation of the black dashed box.

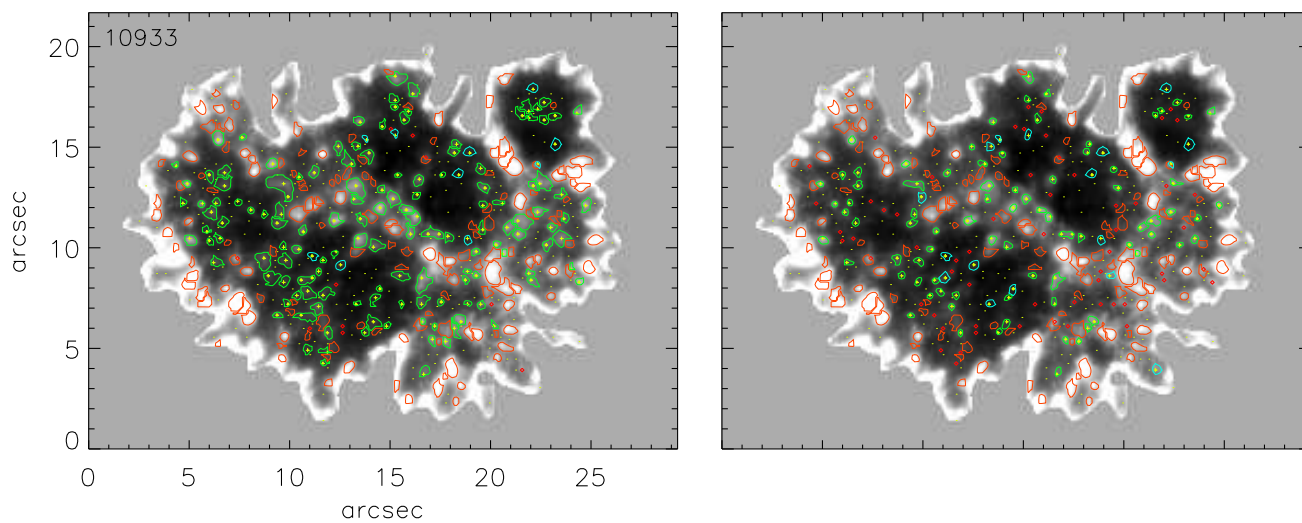


Figure 4. Same as Fig. 3 but for AR 10933.

UDs detected by the two schemes differ nearly entirely

in the green contours and only marginally in the cyan

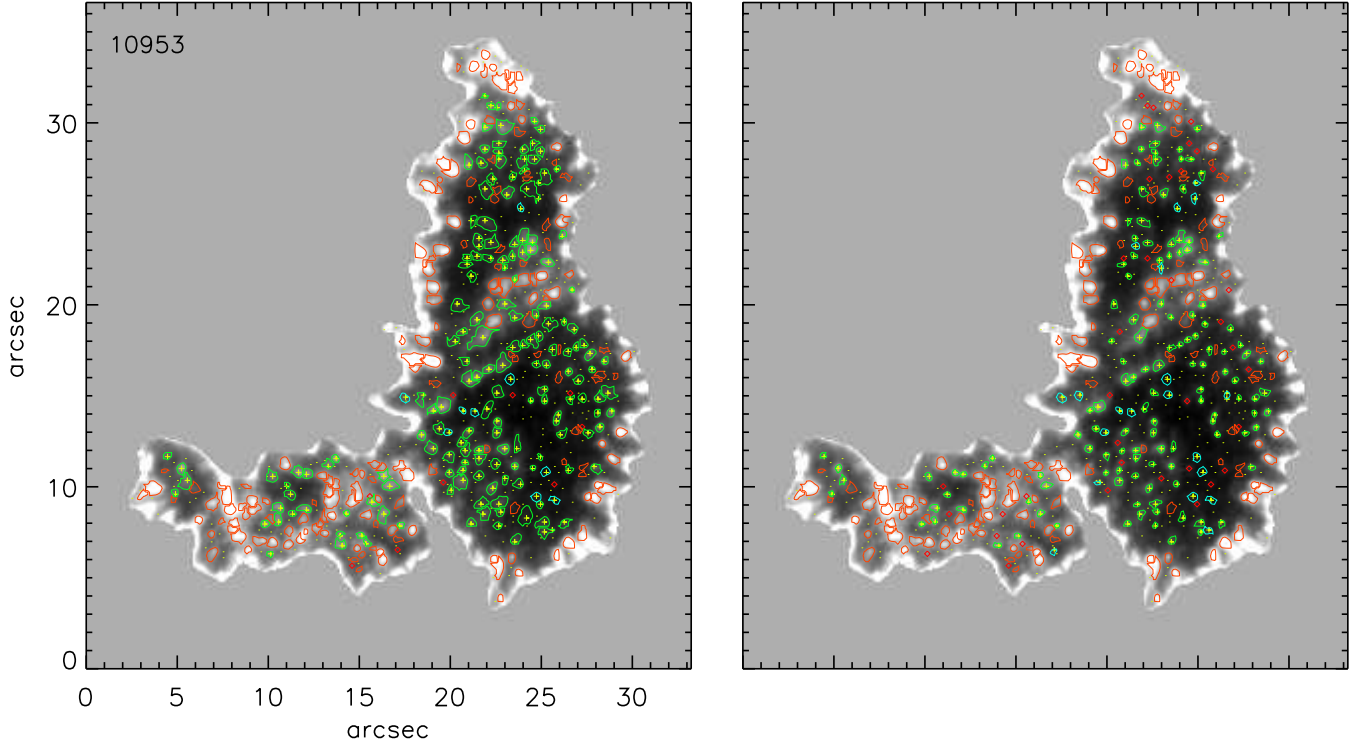


Figure 5. Same as Fig. 4 but for AR 10953.

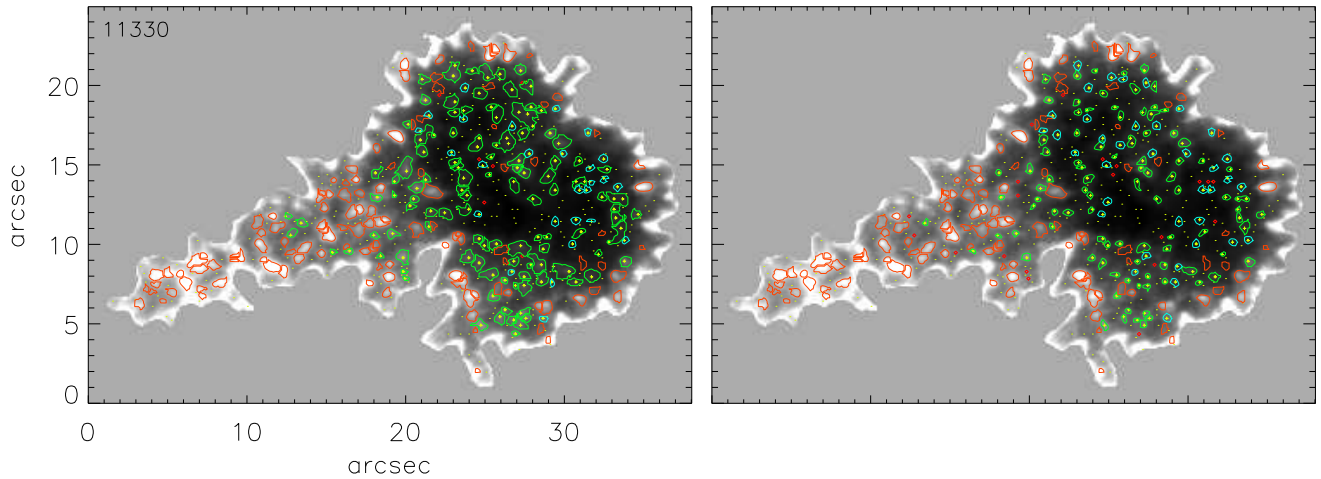


Figure 6. Same as Fig. 5 but for AR 11330.

contours, which correspond to contours labeled “B” and “C”, respectively, with the regular scheme identifying more structures in the green contours than the modified scheme. The green and cyan contours enclose UD that are located in the relatively dark or diffuse regions of the umbra, often in the spaces between brighter UD or on the flanks of light bridges. In addition, the figures

also show that the green contours in the regular scheme tend to be larger than their counterparts in the modified scheme due to the threshold value corresponding to 50% of the sum of the maximum and background intensity. The difference in the number of UD detected by the two schemes with respect to the regular MLT scheme is less than 10% for ARs 10923, 10953, and 11330, while it is

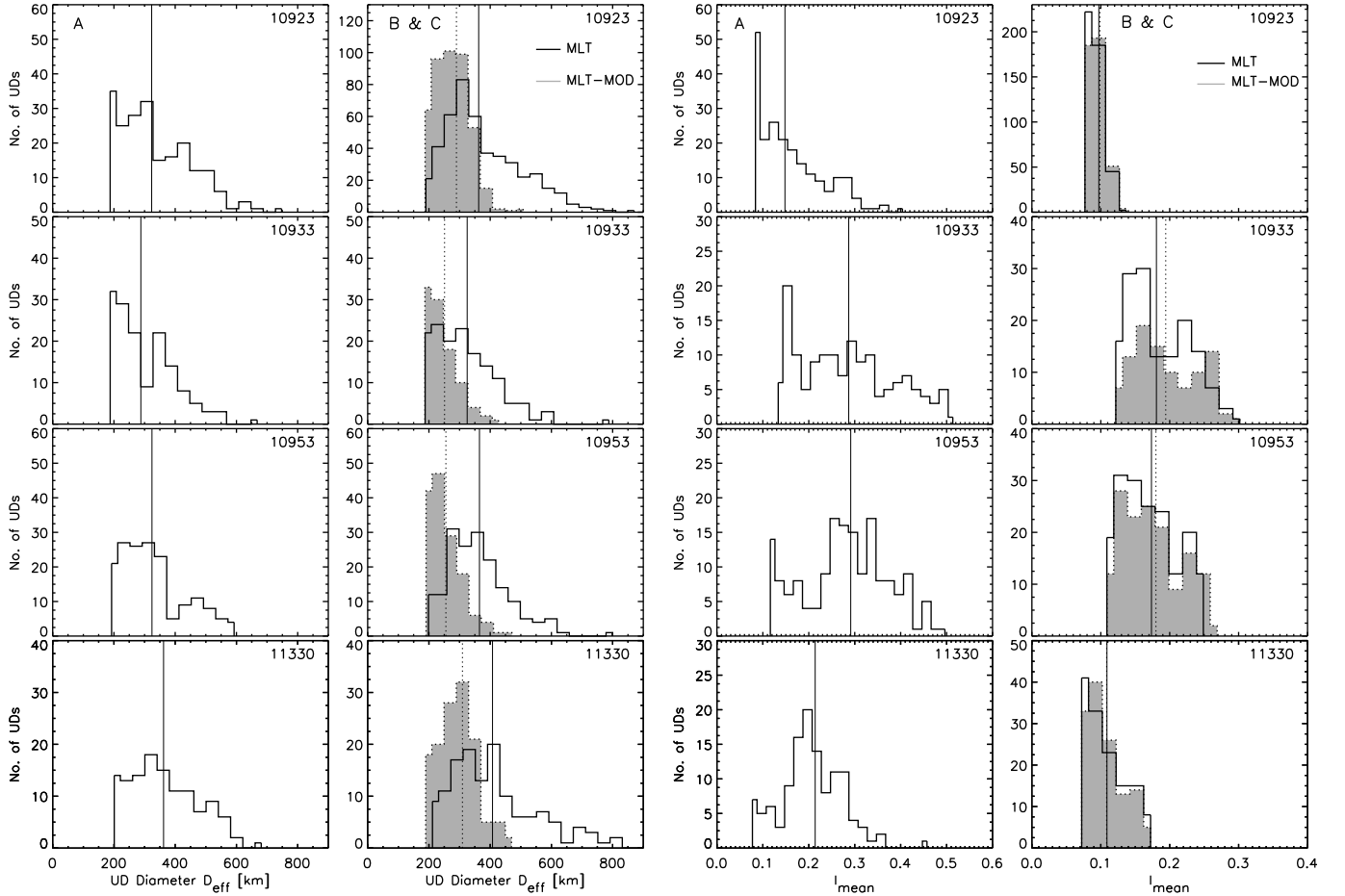


Figure 7. Distribution of effective diameter (columns 1 and 2) and mean intensity (columns 3 and 4) of UDs. The left column corresponds to the red contours, labeled “A”, while the right column corresponds to the green and cyan contours, labeled “B” and “C”, respectively. The black open and gray shaded histograms correspond to the quantities derived using the regular and modified MLT scheme, respectively. A bin size of 40 km and 0.02 was used in the histograms of the effective diameter and mean intensity, respectively.

around 16% for AR 10923. Some contours, specifically the “A”-labeled ones, can appear stacked in succession, as shown in the black dashed box in Fig. 3. An inset of this region shown on the left indicates that it is due to multiple structures that appear alongside each other which is an indication that the MLT detection is not spurious. In the following sections, we will refer either to the color or labels of the contours analogously.

4.2. Physical Characteristics of UDs

Figure 7 shows the histograms for the effective diameter (D_{eff}) and mean intensity (I_{mean}) for the contours labeled “A” (left) and those labeled “B” and “C” (right). The median value of D_{eff} varies between 290–360 km for the contours labeled “A”, with the majority of UDs in all ARs having a value less than 400 km. However, for UDs enclosed by contours “B” and “C”, there is a clear distinction in the distribution as retrieved by the regular

(open; solid) and modified MLT scheme (dark shaded; dotted). The median values obtained by the regular scheme are on average 70–90 km greater than those obtained by the modified scheme, and the histograms tend to extend beyond 400 km, but the number of UDs with $D_{\text{eff}} > 600$ km is less than 10, as seen in ARs 10923 and 11330. The histogram of D_{eff} for contours “B” and “C” from the modified scheme is relatively narrow and confined to a range of about 200–400 km, with median values ranging between 250 and 310 km for the four sunspots. On the other hand, the median values of D_{eff} for the contours labeled “B” and “C” vary from 320 to 410 km for the regular scheme and are on average 40 km larger than UDs enclosed by contours labeled “A”. If one considers all contours combined, then the median value of D_{eff} from the regular approach is around 50 km larger than those retrieved by the modified approach.

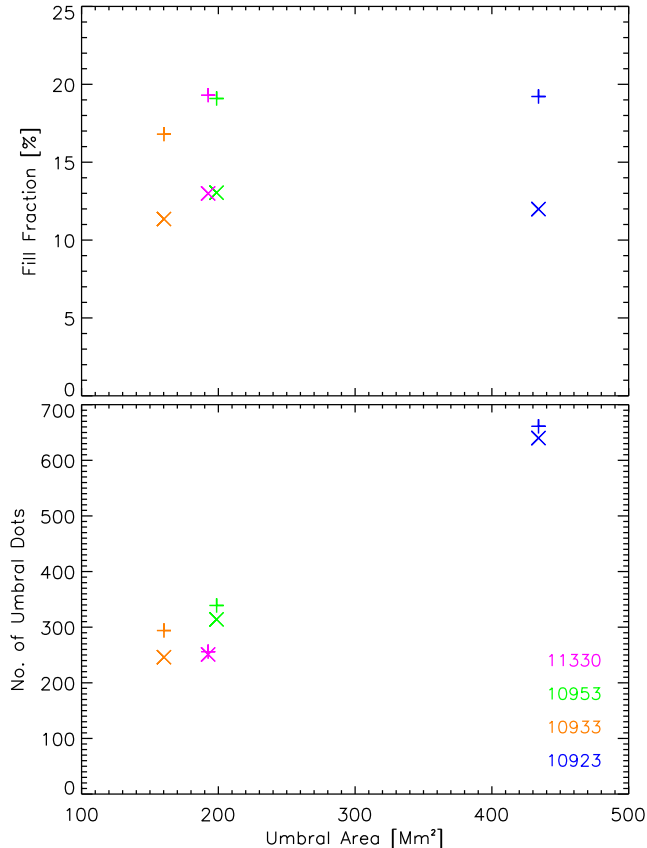


Figure 8. Variation of the UD fill fraction and number as a function of umbral area. The plus and cross symbols refer to the quantities derived from the regular and modified MLT scheme, respectively.

The histograms of the mean intensity (I_{mean}) of UDs enclosed by the red contours (column 3) tend to vary with the sunspots, with a central peak seen in ARs 10953 and 11330, while AR 10923 and 10933 show a large population of fainter UDs. The range of intensities is also different for the four spots, with values extending up to 0.45 for ARs 10933 and 10953, while it is confined to about 0.3 for ARs 10923 and 11330. The median values range from 0.15 in AR 10923 to 0.29 in ARs 10933 and 10953. On the other hand, the histograms of the mean intensity of UDs enclosed by the green and cyan contours (column 4) for both MLT schemes are nearly identical and tend to be narrow, as seen in ARs 10923 and 11330, or extended, as in ARs 10933 and 10953. The median values of the mean intensity for UDs within contours labeled “B” and “C” vary from 0.1–0.19, but are nearly the same for both MLT schemes, with the exception of AR 10933, where only the histogram amplitudes differ between the two approaches.

The quantity $I_{\text{max}}/I_{\text{bck}}$ exhibits an extended histogram (not shown) ranging between 1.02 and 2.5 with median

values ranging between 1.42 and 1.62 for the UDs enclosed by the contours labeled “A”. Unlike D_{eff} , the histograms of $I_{\text{max}}/I_{\text{bck}}$ for UDs enclosed by contours labeled “B” and “C”, are nearly identical for both the regular and modified MLT schemes, with only AR 10933 showing a difference in values around 1.2–1.5 but with a nearly identical shape. The differences in the median values for both schemes vary between 1.2 and 1.43, and the difference is less than 10%.

Figure 8 shows the variation of the fill fraction and number of UDs with the area of the umbral core. The fill fraction is obtained as the ratio of the total area enclosed by the UD contours to the umbral area expressed as a percentage. The plus symbols correspond to the regular MLT scheme where the fill fraction varies from 17 to 19%, while the cross symbols correspond to the modified MLT scheme where the values range from 12 to 13%. The fill fraction obtained from both schemes is thus independent of the umbral area. The number of UDs on the other hand exhibits a very strong correlation with the umbral area, with a linear correlation coefficient of 0.98 and 0.99 for the regular and modified schemes, respectively.

4.3. Density-based Clustering of UDs

In this section, we look at the differences in the clustering of UDs identified by the two MLT schemes. As discussed in Sect. 3.2, DBSCAN requires two parameters, namely, ϵ and M to cluster the data into core, border, and noise points. In order to choose the optimal combination of these two parameters, the routine was run by varying ϵ from 10 to 20 pixels in steps of 0.1 pixel and M from 4 to 10 points in steps of 1 unit. The results obtained from this parameter space are shown in Figs. 9 and 10. It is seen that the number of clusters decreases monotonically with increasing ϵ (top panel) when the value of M is between 4 and 6 points. For higher M values, the number of clusters increases and then decreases with increasing ϵ values, with the maximum number of clusters reducing with increasing M values. The bottom panels of the figures show that the number of noise points monotonically decreases with ϵ , while lower values of M have a smaller number of noise points compared to higher M values for a given ϵ value. The dotted line in the bottom panel indicates the 10% level of all data points for the sunspot, which is used to ascertain the optimum value of ϵ and M for which there are a sufficient number of clusters, which is also verified visually. With this approach, we obtain a range of ϵ values between 10.5 and 11.5 pixels and M between 4 and 5 points. The choice of ϵ and M values produces nearly identical results in the number

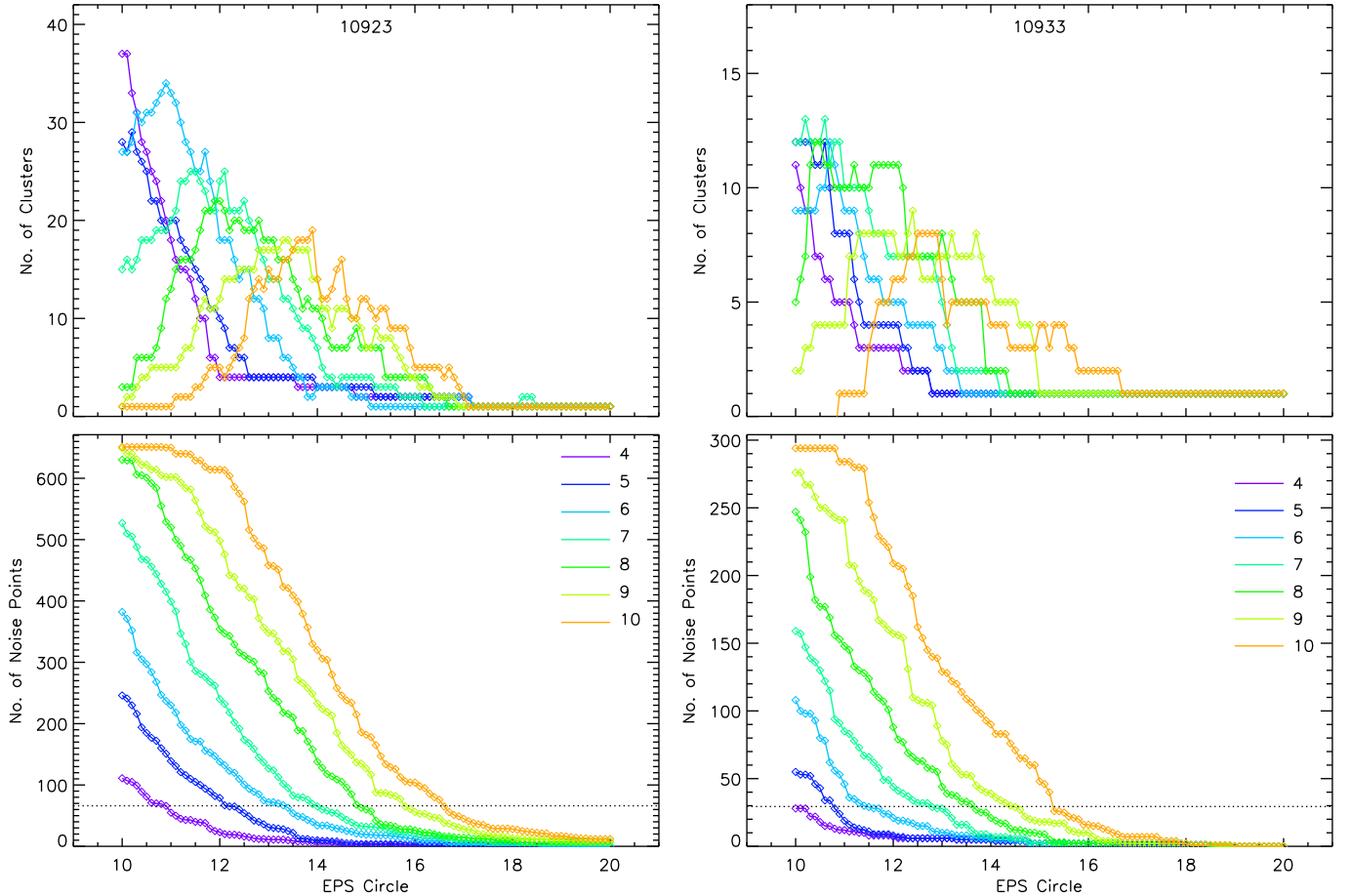


Figure 9. Variation of the number of clusters (top) and noise points (bottom) with the eps circle (ϵ). The different colors correspond to the min. points (M). The left and right columns correspond to AR 10923 and 10933, respectively. The dotted line in the bottom panels represents 10% of the total data points (UD centroids), which is five units less than the maximum value on the y -axis.

of clusters as well as noise points for the regular and modified MLT approach. This is illustrated in Figs. 11 and 12 where the colors indicate the cluster number. The number of clusters obtained for NOAA AR 10923, 10933, 10953, and 11330 are 18(17), 11(12), 10(11), and 11(11) for the regular(modified) MLT scheme, respectively. Similarly, the number of noise points for the four sunspots are 55(57), 43(41), 19(26), and 22(26) for the regular(modified) MLT scheme, respectively.

Figure 11 shows that there is an inhomogeneous distribution of UDs with a preferential clustering in certain regions or locations in the umbra versus others. For instance, in AR 10923, clusters 2 and 6 (top-left panel) and clusters 1 and 5 (top-right panel) are located on opposite sides of the umbra along the major axis of the spot. Clusters 2 (left) and 1 (right) also include a light bridge and other UDs in its vicinity. Clusters 1 (bottom left) and 2 (bottom right) in AR 10933 dominate the western side of the sunspot, while clusters 6 (bottom left) and 7 (bottom right) are co-spatial with a light bridge. A simi-

lar trend is seen in AR 10953 (top panels of Fig. 12) with clusters 1, 6, and 8 using both MLT methods, while cluster 2 is exclusively located in the smaller umbral core in the southeastern part of the spot. The preferential clustering of UDs in the narrower regions of the umbra is also seen in AR 11330; however, in the regular method (bottom-left panel), cluster 3 occupies nearly the entire eastern core with a smaller contribution from cluster 2, while in the modified method, the same region comprises seven smaller clusters, namely, 2, 3, 5, 6, 7, 8, and 9. On the other hand, the clustering in the larger umbral core exhibits a reversed trend where the regular method is associated with nine clusters (bottom-left panel) while the modified method shows only four clusters. It is also seen that the fraction of core and border points with more than 10 UDs in a cluster accounts for more than 70% of all UDs. The number of clusters where there are more than 10 UDs in each cluster varies from four in AR 11330 to eight in AR 10923. The fraction of clusters with 10 UDs or more shows a linear correlation coef-

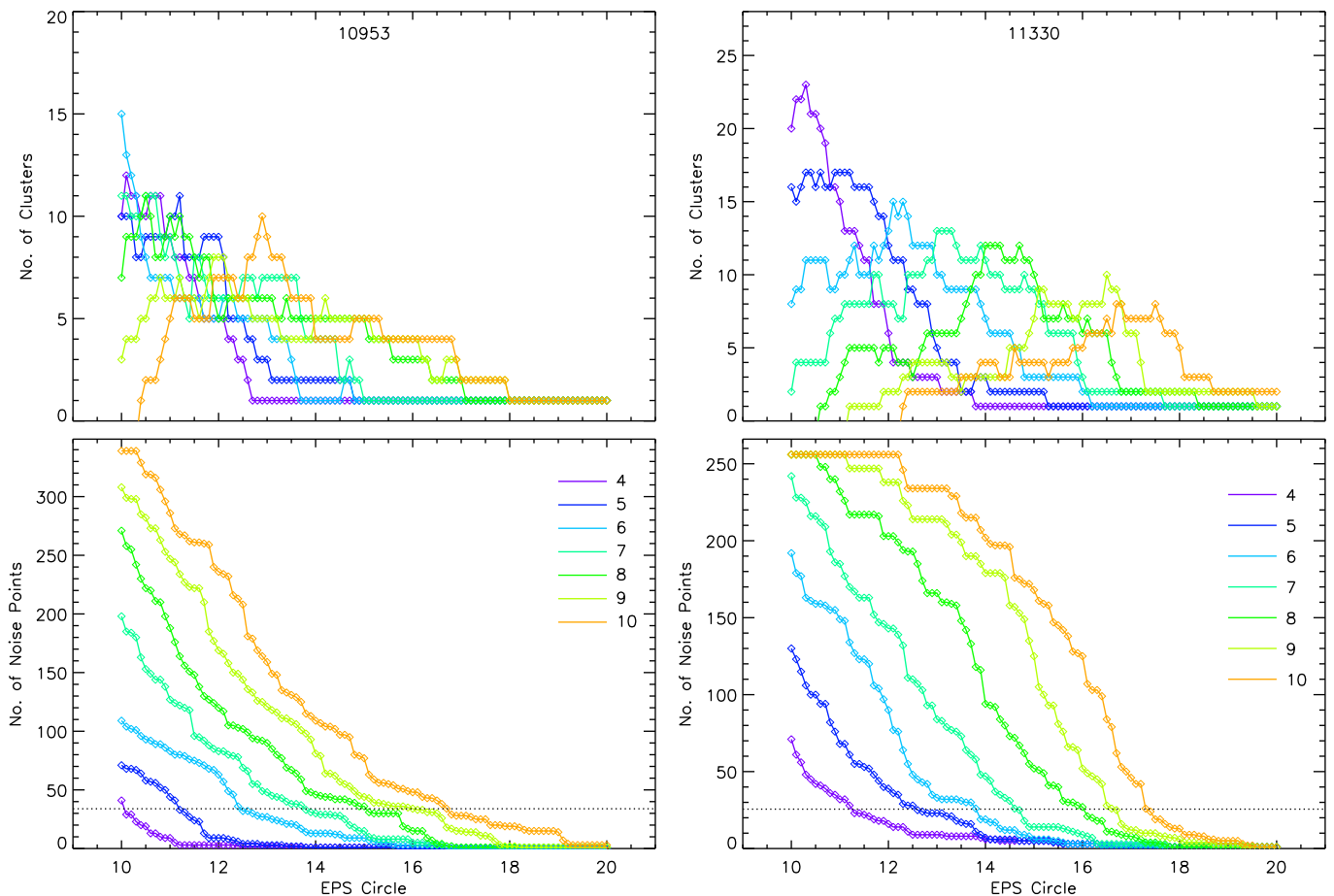


Figure 10. Same as Fig. 9 but for AR 10953 (left) and 11330 (right).

ficient of 0.49 and 0.89 with the sunspot area for the regular and modified MLT approach, respectively. The noise points (red diamonds) are mostly distributed near the umbra-penumbra boundary.

5. DISCUSSION

In this article, we describe two approaches to the MLT method, which is often utilized in the detection of sunspot UDs, and ascertain the resulting differences in the physical quantities arising from the methods. The two approaches differ in the contour level within a patch that encloses a UD – in the first regular method, the level is set at the average of the maximum intensity and background intensity of the patch, i.e., the full-width-at-half-maximum, while in the second modified method, the level is set at the average of the maximum intensity and mean intensity of the patch. In the modified approach, there can be multiple contours that enclose pixels with a local intensity maxima, while in the regular approach, there is only one contour. While both approaches differ in the contour level and the number of contours within an MLT patch, we also restrict the points of local intensity maxima as those

having a value greater than 30% of the minimum umbral intensity and less than the mean intensity of all remaining pixels of local maxima. As a consequence of the above, the median effective diameter from the regular approach is about 70–90 km greater than that from the modified approach, where the median values range from 320 to 410 km with the regular method. The larger effective diameter retrieved by the regular approach also yields a fill fraction that is around 6% higher on average for all sunspots, as compared to those retrieved from the modified approach. The differences in the effective diameter are, however, within the spatial sampling of the Hinode blue continuum images and also consistent with earlier quoted values (M. Sobotka et al. 1997b; A. Tritschler & W. Schmidt 2002; M. Sobotka & K. G. Puschmann 2009; M. Sobotka & J. Jurčák 2009; H. Watanabe et al. 2009; R. E. Louis et al. 2012; H. Watanabe et al. 2012). The values of the fill fraction from both methods are also in agreement with previously reported values (M. Sobotka et al. 1997b; A. Tritschler & W. Schmidt 2002; R. Yadav et al. 2018). On the other hand, the histograms of the mean intensity are nearly identical for

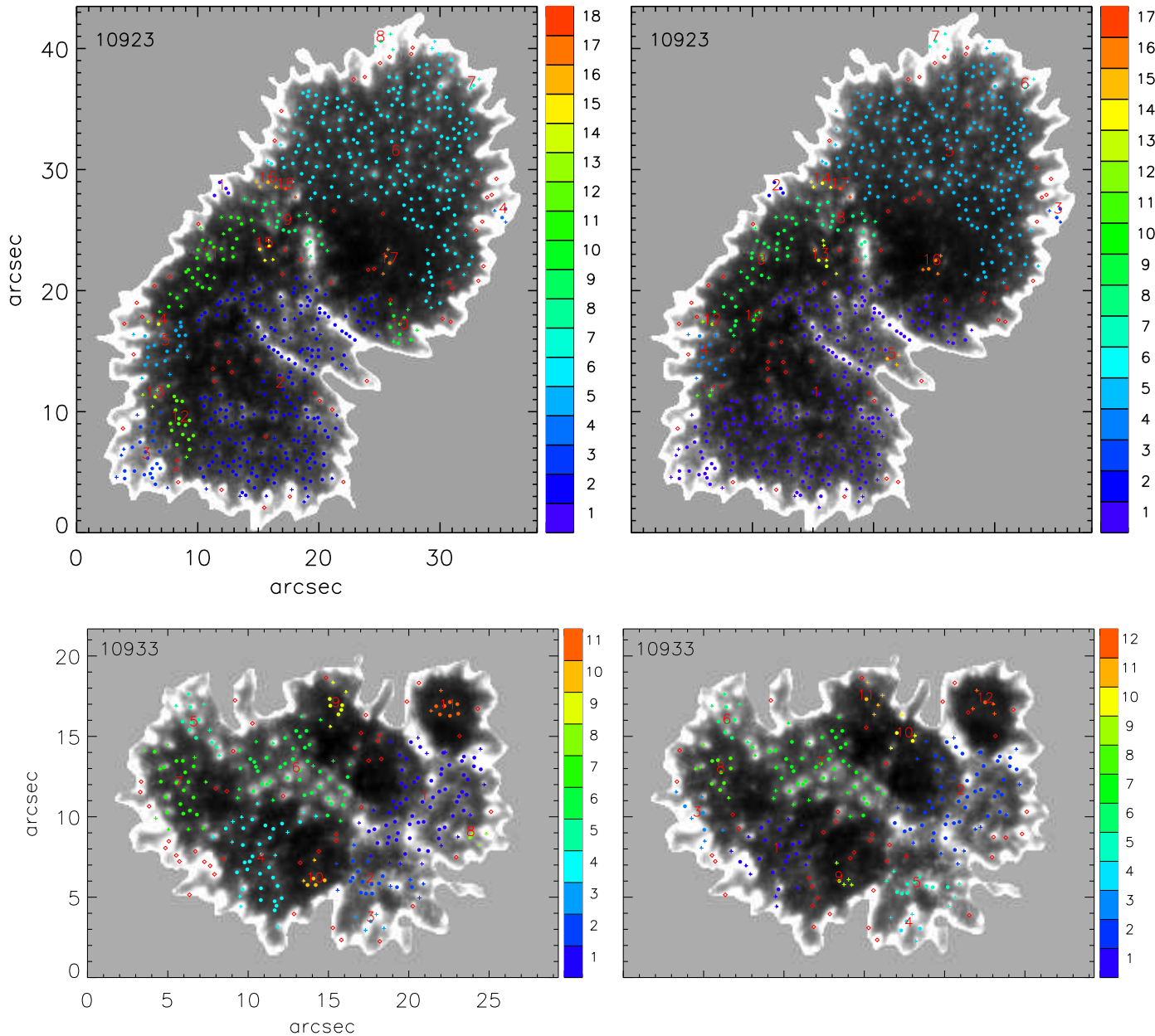


Figure 11. Clustering of UD's derived from DBSCAN. The colored filled circles represent core points, as indicated in the legend on the right, while the plus symbols represent border points. The red diamonds correspond to noise points. The top panels correspond to AR 10923, with the left and right panel showing the clustering with the regular and modified MLT scheme, respectively. Bottom panels: same as the top panels but for AR 10933.

both approaches, with only AR 10933 showing a small difference in the amplitude. Similarly, the density-based, spatial clustering of UD's from both approaches yields very similar results in terms of the number of clusters and noise points. The ϵ and M values used in the clustering routine for both methods are within two pixels. Thus, the inclusion of points of local maxima

along with MLT does not produce significant differences statistically.

We finally comment on the spatial clustering of UD's in the context of MHD simulations of magneto-convection in sunspots. *M. Schüssler & A. Vögler (2006)* showed that the $\tau = 1$ surface is elevated by around 300 km at the location of the convective plume, corresponding to the UD where the upflows are the strongest and the

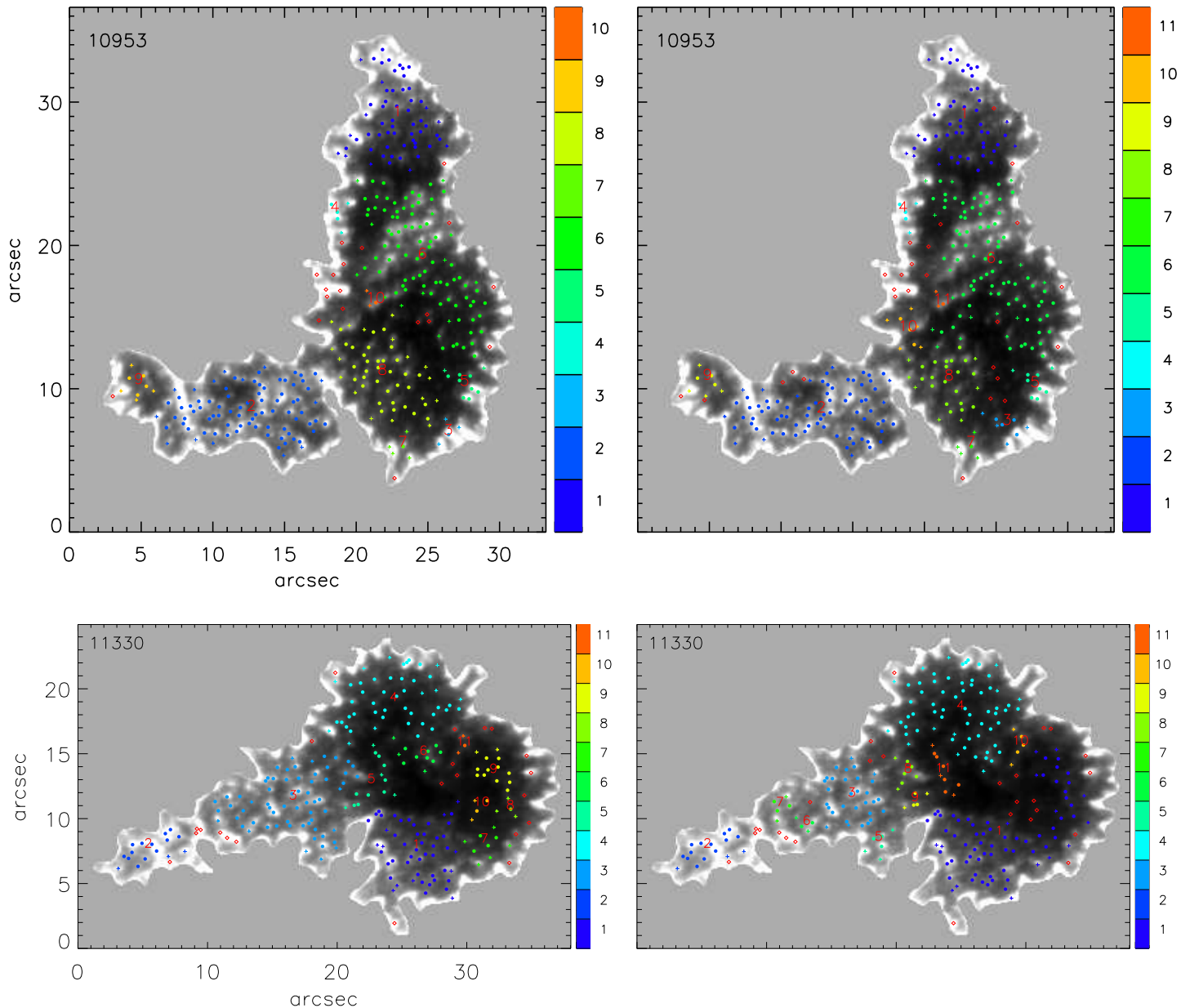


Figure 12. Same as Fig. 11 but for AR 10953 (top) and AR 11330 (bottom).

magnetic field is significantly reduced in comparison to the surroundings. However, the contrast in the velocity and magnetic signatures of the UD is significantly reduced with respect to the adjacent umbra as one goes higher to $\tau = 0.1$ and 0.01 , where most spectral lines form. The typical vertical extension of UD varies between 0.6 and 0.9 Mm during their temporal evolution (M. Schüssler & A. Vögler 2006). While UD are shallow and mostly, sub-photospheric phenomena, their spatial distribution within the umbra depends on the field strength and in particular its vertical component, which

dictates whether a fluid parcel will be convectively stable (D. O. Gough & R. J. Tayler 1966). This is particularly evident in numerical simulations of a pair of opposite-polarity sunspots adjacent to each other with field strengths of 3 and 4 kG (M. Rempel et al. 2009; M. Rempel 2011), where the inhomogeneous clustering of UD in the sunspot with a lower field strength is consistent with our results shown in Figs. 11 and 12. A point to be noted is that while radiative MHD simulations provide three-dimensional cubes of physical quantities such as the vector magnetic field, velocity, temper-

ature, pressure, and density, etc., they do not provide a mask for the locations of UDs, which would permit an absolute ground truth to compare with observations. In addition, the sunspot fine structure in the visible photospheric layers where spectral lines typically form is sensitive to the boundary conditions used in the MHD framework that can produce significant variations in the spatial and photometric distribution of UDs, as described above. Thus, while comparisons between different tracking methods are possible, ascertaining a superior routine is possible only when the quantities are known a priori. The preferential regions in the umbra, where UDs are populous, would suggest that the classical categorization of UDs as peripheral and central, based on their proximity to the umbra-penumbra boundary, requires a reconsideration. While we have presented only four sunspots in this article, we plan to extend our clustering analysis to a larger sample of spots at different evolutionary stages, in-situ conditions, morphologies, and magnetic complexities. This would permit a better understanding of the conditions that lead to a localization of convective intrusions within a sunspot umbra that can be compared with numerical simulations.

6. CONCLUSIONS

The modification of the standard MLT routine, used in the detection of sunspot UDs, to include local intensity enhancements produces a smaller effective diameter within the range of 70–90 km and a reduced fill fraction of around 6% in comparison to the regular scheme. However, these differences are still within the range of values cited by earlier works. On the other hand, the distribution of the mean intensity of UDs from both methods is nearly identical. A density-based spatial clustering of

the UDs also shows similar results with both detection routines. In addition, there is a preferential clustering of UDs in the umbra, particularly in the vicinity of faint light bridges or where the umbral core is constricted. Further analysis is required to ascertain the dependency of the clustering of UDs with the in-situ and external environment of the sunspot and include the clustering to time-dependent quantities such as horizontal speeds and lifetimes, etc. An absolute ground truth is essential to clarify which tracking routine is superior; however the unique intrinsic magnetic environment of an AR, renders such a distinction, non-trivial.

ACKNOWLEDGMENTS

Hinode is a Japanese mission developed and launched by ISAS/JAXA, collaborating with NAOJ as a domestic partner, NASA and STFC (UK) as international partners. Scientific operation of the *Hinode* mission is conducted by the *Hinode* science team organized at ISAS/JAXA. This team mainly consists of scientists from institutes in the partner countries. Support for the post-launch operation is provided by JAXA and NAOJ (Japan), STFC (UK), NASA, ESA, and NSC (Norway). We thank the referee for providing insightful and useful comments.

AUTHOR CONTRIBUTIONS

R.E.L formulated the idea, compiled the MLT and DB-SCAN routines in IDL, performed the analysis, and wrote the manuscript. A.C. selected the *Hinode* observations and reduced the data.

REFERENCES

- Barrodale, I., Skea, D., Berkley, M., Kuwahara, R., & Poeckert, R. 1993, *Pattern Recognition*, 26, 375, doi: [10.1016/0031-3203\(93\)90045-X](https://doi.org/10.1016/0031-3203(93)90045-X)
- Beckers, J. M., & Schröter, E. H. 1968, *SoPh*, 4, 303, doi: [10.1007/BF00149561](https://doi.org/10.1007/BF00149561)
- Bharti, L., Beeck, B., & Schüssler, M. 2010, *A&A*, 510, A12, doi: [10.1051/0004-6361/200913328](https://doi.org/10.1051/0004-6361/200913328)
- Biermann, L. 1941, *Vierteljahresschrift der Astronomischen Gesellschaft*, 76, 194
- Bovelet, B., & Wiehr, E. 2001, *SoPh*, 201, 13, doi: [10.1023/A:1010344827952](https://doi.org/10.1023/A:1010344827952)
- Chitre, S. M. 1963, *MNRAS*, 126, 431, doi: [10.1093/mnras/126.5.431](https://doi.org/10.1093/mnras/126.5.431)
- Choudhuri, A. R. 1986, *ApJ*, 302, 809, doi: [10.1086/164042](https://doi.org/10.1086/164042)
- Danielson, R. E. 1964, *ApJ*, 139, 45, doi: [10.1086/147738](https://doi.org/10.1086/147738)
- Deinzer, W. 1965, *ApJ*, 141, 548, doi: [10.1086/148144](https://doi.org/10.1086/148144)
- Gough, D. O., & Tayler, R. J. 1966, *MNRAS*, 133, 85, doi: [10.1093/mnras/133.1.85](https://doi.org/10.1093/mnras/133.1.85)
- Grossmann-Doerth, U., Schmidt, W., & Schroeter, E. H. 1986, *A&A*, 156, 347
- Hamedivafa, H. 2008, *SoPh*, 250, 17, doi: [10.1007/s11207-008-9201-0](https://doi.org/10.1007/s11207-008-9201-0)
- Kosugi, T., Matsuzaki, K., Sakao, T., et al. 2007, *SoPh*, 243, 3, doi: [10.1007/s11207-007-9014-6](https://doi.org/10.1007/s11207-007-9014-6)
- Liao, P.-S., Chen, T.-S., Chung, P.-C., et al. 2001, *J. Inf. Sci. Eng.*, 17, 713
- Loughhead, R. E., Bray, R. J., & Tappere, E. J. 1979, *A&A*, 79, 128

- Louis, R. E., Mathew, S. K., Bellot Rubio, L. R., et al. 2012, *ApJ*, 752, 109, doi: [10.1088/0004-637X/752/2/109](https://doi.org/10.1088/0004-637X/752/2/109)
- Louis, R. E., Mathew, S. K., & Raja Bayanna, A. 2024, *Advances in Space Research*, 73, 3256, doi: [10.1016/j.asr.2023.12.046](https://doi.org/10.1016/j.asr.2023.12.046)
- Meister, A. L. F. 1769, *Nov. Com. Gött.*, 1, 144
- Ortiz, A., Bellot Rubio, L. R., & Rouppe van der Voort, L. 2010, *ApJ*, 713, 1282, doi: [10.1088/0004-637X/713/2/1282](https://doi.org/10.1088/0004-637X/713/2/1282)
- Otsu, N. 1979, *IEEE Transactions on Systems, Man, and Cybernetics*, 9, 62, doi: [10.1109/TSMC.1979.4310076](https://doi.org/10.1109/TSMC.1979.4310076)
- Parker, E. N. 1979, *ApJ*, 234, 333, doi: [10.1086/157501](https://doi.org/10.1086/157501)
- Rempel, M. 2011, *ApJ*, 729, 5, doi: [10.1088/0004-637X/729/1/5](https://doi.org/10.1088/0004-637X/729/1/5)
- Rempel, M., Schüssler, M., Cameron, R. H., & Knölker, M. 2009, *Science*, 325, 171, doi: [10.1126/science.1173798](https://doi.org/10.1126/science.1173798)
- Riethmüller, T. L., Solanki, S. K., Zakharov, V., & Gandorfer, A. 2008, *A&A*, 492, 233, doi: [10.1051/0004-6361:200810701](https://doi.org/10.1051/0004-6361:200810701)
- Rimmele, T. 2008, *ApJ*, 672, 684, doi: [10.1086/523702](https://doi.org/10.1086/523702)
- Sainz Dalda, A., de la Cruz Rodríguez, J., De Pontieu, B., & Gošić, M. 2019, *ApJL*, 875, L18, doi: [10.3847/2041-8213/ab15d9](https://doi.org/10.3847/2041-8213/ab15d9)
- Schüssler, M., & Vögler, A. 2006, *ApJL*, 641, L73, doi: [10.1086/503772](https://doi.org/10.1086/503772)
- Sobotka, M., Brandt, P. N., & Simon, G. W. 1997a, *A&A*, 328, 689
- Sobotka, M., Brandt, P. N., & Simon, G. W. 1997b, *A&A*, 328, 682
- Sobotka, M., & Jurčák, J. 2009, *ApJ*, 694, 1080, doi: [10.1088/0004-637X/694/2/1080](https://doi.org/10.1088/0004-637X/694/2/1080)
- Sobotka, M., & Puschmann, K. G. 2009, *A&A*, 504, 575, doi: [10.1051/0004-6361/200912365](https://doi.org/10.1051/0004-6361/200912365)
- Tritschler, A., & Schmidt, W. 2002, *A&A*, 388, 1048, doi: [10.1051/0004-6361:20020542](https://doi.org/10.1051/0004-6361:20020542)
- Tsuneta, S., Ichimoto, K., Katsukawa, Y., et al. 2008, *SoPh*, 249, 167, doi: [10.1007/s11207-008-9174-z](https://doi.org/10.1007/s11207-008-9174-z)
- Viticchié, B., & Sánchez Almeida, J. 2011, *A&A*, 530, A14, doi: [10.1051/0004-6361/201016096](https://doi.org/10.1051/0004-6361/201016096)
- Watanabe, H., Bellot Rubio, L. R., de la Cruz Rodríguez, J., & Rouppe van der Voort, L. 2012, *ApJ*, 757, 49, doi: [10.1088/0004-637X/757/1/49](https://doi.org/10.1088/0004-637X/757/1/49)
- Watanabe, H., Kitai, R., & Ichimoto, K. 2009, *ApJ*, 702, 1048, doi: [10.1088/0004-637X/702/2/1048](https://doi.org/10.1088/0004-637X/702/2/1048)
- Weiss, N. O., Brownjohn, D. P., Hurlburt, N. E., & Proctor, M. R. E. 1990, *MNRAS*, 245, 434, doi: [10.1093/mnras/245.3.434](https://doi.org/10.1093/mnras/245.3.434)
- Yadav, R., Louis, R. E., & Mathew, S. K. 2018, *ApJ*, 855, 8, doi: [10.3847/1538-4357/aaaeba](https://doi.org/10.3847/1538-4357/aaaeba)